Integration of Yagi antenna in LTCC package for differential 60-GHz radio

Gaucher, B. P.; Wai, L. L.; Zhang, Yue Ping; Sun, Mei; Liu, Duixian; Chua, Kai Meng

2008

Zhang, Y. P., Gaucher, B. P., Sun, M., Liu, D., Wai, L. L., & Chua, K. M. (2008). Integration of Yagi antenna in LTCC package for differential 60-GHz radio. IEEE Transactions on Antennas and Propagation. 56(8), 2780-2783.

https://hdl.handle.net/10356/93099

https://doi.org/10.1109/TAP.2008.927577

[16] R. Carriere and R. L. Moses, "High resolution radar target modeling using a modified Prony estimator," *IEEE Trans. Antennas Propag.*, vol. 40, no. 1, pp. 13–18, Jan. 1992.
[17] R. C. Qiu and I.-T. Lu, "Multipath resolving with frequency dependence for wide-band wireless channel modeling," *IEEE Trans. Veh. Technol.*, vol. 28, no. 1, pp. 273–285, Jan. 1999.
[18] L. C. Potter, D.-M. Chiang, R. Carriere, and M. J. Gerry, "A GTD-based parametric model for radar scattering," *IEEE Trans. Antennas Propag.*, vol. 43, no. 10, pp. 1058–1067, Oct. 1995.
[19] A. Papoulis, *Probability, Random Variables, and Stochastic Processes*, 3rd ed. New York: McGraw-Hill, 1991.
[20] A. D. Whalen, *Detection of Signals in Noise*, 1st ed. Boston, MA: Academic Press, 1971.
[21] R. Luebbers, "Finite conductivity uniform GTD versus knife edge diffraction in prediction of propagation path loss," *IEEE Trans. Antennas Propag.*, vol. 32, no. 1, pp. 70–76, Jan. 1984.
[22] [Online]. Available: http://cm.bell-labs.com/cm/cs/who/bwk/wise/index.html
[23] V. Erceg, S. Fortune, J. Ling, A. Rustako, and R. Valenzuela, "Comparisons of a computer-based propagation prediction tools with experimental data collected in urban microcellular environments," *IEEE J. Sel. Areas Commun.*, vol. 15, pp. 677–684, May 1997.
[24] D. Ullmo and H. U. Baranger, "Wireless propagation in buildings: A statistical scattering approach," *IEEE Trans. Veh. Technol.*, vol. 48, no. 3, pp. 947–955, May 1999.
[25] F. A. Agelet, A. Formella, J. M. H. Rabanos, F. I. de Vincente, and F. P. Fontan, "Efficient ray-tracing acceleration techniques for radio propagation modeling," *IEEE Trans. Veh. Technol.*, vol. 49, no. 6, pp. 2089–2104, Nov. 2000.
[26] A. Muqaibel, S.-J. Bayram, A. M. Attiya, and S. M. Riad, "Ultrawideband through-the-Wall propagation," *Proc. Inst. Elect. Eng. Microw., Antennas Propag.*, vol. 152, no. 6, pp. 581–588, Dec. 2005.
[27] F. Sagnard and G. E. Zein, "In situ characterizations of building materials for propagation modeling: Frequency and time responses," *IEEE Trans. Antennas Propag.*, vol. 53, no. 10, pp. 3166–3173, Oct. 2005.
[28] A. Muqaibel, A. Safaai-Jazi, A. Bayram, and S. M. Riad, "Ultra wideband material characterization for indoor propagation," in *Proc. IEEE Antennas and Propagation Society Symp.*, Columbus, OH, Jun. 2003, vol. 4, pp. 623–626.
[29] Y. P. Zhang and Y. Hwang, "Measurements of the characteristics of indoor penetration loss," in *Proc. IEEE Vehicular Technology Conf., Spring*, Stockholm, Sweden, Jun. 1994, vol. 3, pp. 1741–1744.
[30] G. German, Q. Spencer, L. Swindlehurst, and R. Valenzuela, "Wireless indoor channel modeling: Statistical agreement of ray tracing simulations and channel sounding measurements," in *Proc. IEEE Conf. on Acoustics, Speech, and Signal Processing*, Salt Lake City, UT, May 2001, vol. 4, pp. 2501–2504.
[31] J. Kraus, *Electromagnetics*, 3rd ed. New York: McGraw-Hill, 1984.

Integration of Yagi Antenna in LTCC Package for Differential 60-GHz Radio

M. Sun, Y. P. Zhang, K. M. Chua, L. L. Wai, D. Liu, and B. P. Gaucher

***Abstract*—A Yagi antenna implemented in a thin cavity-down ceramic ball grid array package in low temperature cofired ceramic (LTCC) technology is reported. The antenna, intended for use in highly integrated differential 60-GHz radios, has achieved a 10-dB impedance bandwidth of 2.3 GHz from 60.6 to 62.9 GHz and a peak gain of 6 dBi at 62 GHz.**

***Index Terms*—60-GHz radio, antenna-in-package (AiP), low temperature cofired ceramic (LTCC).**

I. Introduction

An IEEE standards group 802.15.3c is defining specifications for 60-GHz radio to use a few Gigahertz of unlicensed spectrum to enable very high-data-rate applications, such as high-speed Internet access, streaming content downloads, and wireless data bus for cable replacement. The targeted data rate for these applications is greater than 2 Gb/s [1]. For the 60-GHz radio, in order to have mass deployment and meet consumer marketplace requirements the cost and size of any solution has to be low and compact. In fact, designs towards low-cost highly-integrated 60-GHz radio have been carried out in silicon technologies. For example, Brian, *et al.* demonstrated the first experimental 60-GHz radio transmitter and receiver chipset in a 0.13-μm silicon-germanium (SiGe) technology [2] and Razavi a 60-GHz radio transceiver chip in a 0.13-μm complementary metal oxide semiconductor (CMOS) technology [3]. These highly-integrated 60-GHz radios are designed with differential architectures. A differential architecture is of great advantage in current silicon technology for highly-integrated radios because the differential nature permits higher linearity, lower offset, makes it immune to power supply variations and substrate noise. Thus, exploring the design of differential antenna is essential for these radios to get rid of off-chip or lossy on-chip baluns.

Antenna designs for radio operating at 60 GHz or above are turning to antenna-on-chip (AoC) and antenna-in-package (AiP) solutions [4]–[7]. This is because the antenna form factor at 60 GHz is on the order of millimetres or less, which opens up new integration options on a chip or in a package. Zhang, *et al.* evaluated the AoC solution for 60-GHz radio on a silicon substrate and found that both inverted-F and quasi-Yagi on-chip antennas have very poor radiation efficiency about 5% due to the low resistivity and high permittivity of the silicon substrate [4]. Micromachining techniques and proton implantation process have been proposed to reduce silicon substrate loss so as to improve the AoC radiation efficiency [5], [6]. Pfeiffer, *et al.* demonstrated a complete AiP solution for 60-GHz radio in a plastic land grid array package and a folded dipole (differential) antenna suspended in

Manuscript received October 2, 2007; revised February 27, 2008. Published August 6, 2008 (projected).

M. Sun and Y. P. Zhang are with the School of Electrical and Electronic Engineering, Nanyang Technological University, Singapore 639798, Singapore (e-mail: sunmei@ntu.edu.sg, eypzhang@ntu.edu.sg).

K. M. Chua and L. L. Wai are with the Singapore Institute of Manufacturing Technology, Singapore 638075, Singapore (e-mail: kmchua@SIMTech.a-star.edu.sg).

D. Liu and B. P. Gaucher are with the IBM T. J. Watson Research Center, Yorktown Heights, NY 10598 USA (e-mail: duixian@us.ibm.com).

Color versions of one or more of the figures in this paper are available online at http://ieeexplore.ieee.org.

Digital Object Identifier 10.1109/TAP.2008.927577

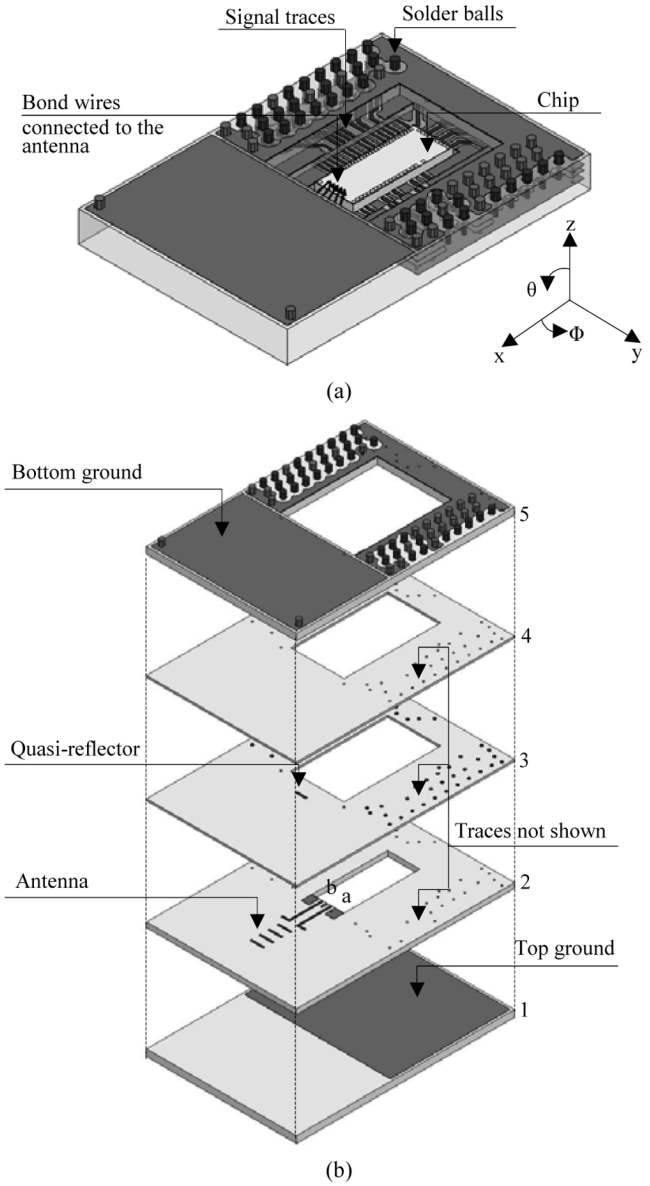

Fig. 1. Yagi AiP: (a) bottom view and (b) explored view.

a metal cavity showed a gain of 7 dBi and a radiation efficiency better than 90% [7]. In this letter we report a Yagi (differential) antenna in a thin cavity-down ceramic ball grid array (CBGA) package realized in low temperature cofired ceramic (LTCC) technology for 60-GHz radio. The LTCC process has recently been added to the narrow list of technologies capable of realizing millimeter-wave wireless systems.

II. Integration of Yagi Antenna in a Package

Fig. 1 shows the configuration of the Yagi AiP for highly integrated 60-GHz radios. The package ceramic material is LTCC ferro-A6 with a relative permittivity and a loss tangent of 5.9 and 0.002, respectively. The package metallic materials are gold and silver. The achievable resolution is 50 μm for line width/space. The size of the entire AiP is $12.5 \times 8.6 \times 1.575$ mm^3. Five ceramic layers are used to form the package. The four cavity layers form a package cavity to hold a radio chip not larger than $4.1 \times 1.6 \times 0.46$ mm^3. Table I lists the thickness and cavity size per layer. The per fired layer thickness tolerance is $\pm 1.5\%$. The accuracy of the process in creating cavity is $+0\%/-2\%$. It should be noted that the 2nd layer has a Yagi driver and four Yagi directors. The 3rd layer has a Yagi quasi-reflector. The 5th layer has a bottom ground, which also functions as a Yagi reflector. It should be noted that the radio chip is adhered to the cavity base of the top ground plane. This configuration will contribute to the shielding of the chip from the antenna [9]. It also helps to dissipate heat better as the top ground plane acts as heatsink. The signals from the chip are connected to the Yagi antenna using bond wires in a ground-signal-ground-signal-ground (G-S-G-S-G) configuration. The other signals from the chip are connected to the outside PCB by the bond wires, signal traces, vias, and solder balls. The ground planes in five layers are all connected by vias and they are also connected to the outside PCB ground by solder balls. This will also help to dissipate heat better.

TABLE I
Dimensions Per Layer

Layers	Thickness in mm	Cavity size in mm^3
1st	0.385	-
2nd	0.285	4.35×1.85×0.285
3rd	0.105	5.55×3.05×0.105
4th	0.105	5.55×3.05×0.105
5th	0.385	5.55×4.25×0.385

The simulations were performed in the XFDTD [8]. The AiP was simulated without chip and bond wires. This facilitates the antenna design and also agrees with our measurement condition. To model the AiP accurately, the spatial step sizes Δx, Δy, and Δz were chosen to be 0.031 mm. Thus, the AiP was fitted with $403 \times 277 \times 51$ cells and also the spatial step sizes were much smaller than $\lambda g/10$ at 55–65 GHz, where λg is the guided wavelength. To calculate the far-field patterns, the additional 20 free space mesh cells were added to all six sides of the AiP. The total computational space was $443 \times 317 \times 91$ cells. In simulation, the differential feeding was realized by inserting two 50-Ù Gaussian pulse voltage sources in the gaps between the ground-signal (G-S) feeding pads of the antenna. The time step in our simulations was $\Delta t = 57.77$ fs, which satisfies the Courant stability criterion. The Gaussian pulse width was 64 time steps. It was found that 5000 time steps were sufficient for convergence in our simulation. For differential antenna design, the differential input impedance Z_d is an important parameter. Its value is required in the design of matching network between the differentially-driven antenna and the differential active circuitry in a radio system. The differentially-driven antenna can be treated as a two-port network. With reference to the ground plane the left driving point at a is defined as port 1 and the right driving point at b as port 2 [as shown in Fig. 1(b)]. Using the S-parameters for ports 1 and 2, one can express the differential input impedance Z_d as [10]

$$Z_d = 2Z_0 \frac{\left(1 - S_{11}^2 + S_{21}^2 - 2S_{21}\right)}{\left(1 - S_{11}\right)^2 - S_{21}^2} \tag{1}$$

where Z_0 is the reference impedance of 50 Ω. The return loss in dB calculated from Z_d is then given by

$$RL = 20 \lg \left| \frac{Z_d - Z_c}{Z_d + Z_c} \right| \tag{2}$$

where Z_c is the reference impedance of 100 Ω.

Fig. 2 shows the layout of the final designed Yagi AiP. The pitch of the G-S-G-S-G feeding pads is 250 μm. The width of the driver, directors, and quasi-reflector has the same value of 0.1 mm. The length of the directors has the same value of $L_{\rm dir}$. $L_{\rm dri}$ is the length of the driver. $L_{\rm ref}$ is the length of the quasi-reflector. $S_{\rm dir}$ is the distance between the neighboring directors, which is equal to the distance between the driver and the first director. $S_{\rm ref}$ is the distance between the driver and the quasi-reflector. Table II lists their dimensions in mm and λg.

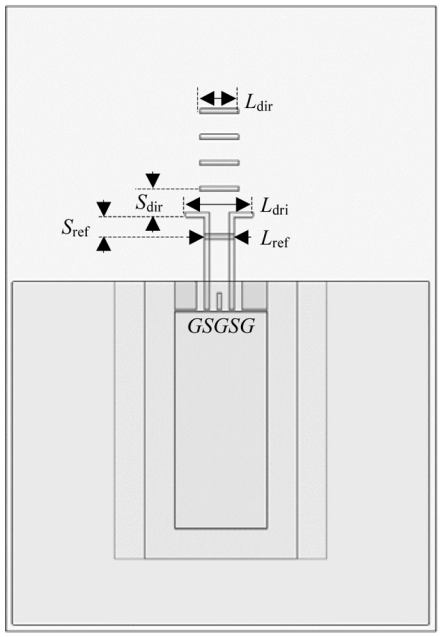

Fig. 2. Yagi AiP layout.

TABLE II
DIMENSIONS IN FIG. 2

	L_{dri}	L_{dir}	L_{ref}	S_{dir}	S_{ref}
in mm	1.36	0.768	0.614	0.518	0.442
in λg	~0.56	~0.32	~0.25	~0.22	~0.18

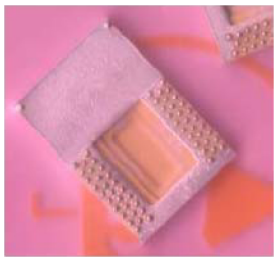

Fig. 3. Photo of the fabricated Yagi AiP.

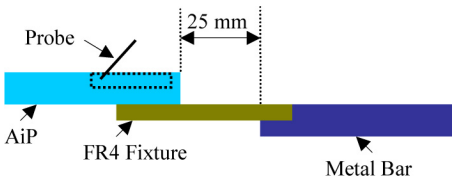

Fig. 4. Measurement set up.

III. RESULTS

Fig. 3 shows the photo of the fabricated Yagi AiP. The S-parameters were measured with a probe based millimeter-wave antenna measurement setup for 50–65 GHz frequency range [11]. As shown in Fig. 4, the AiP is supported by an FR4 fixture. This provides the good support for probe touching the G-S-G-S-G feeding pads for measurement. This will also avoid the direct contact of the AiP on the metal probe station. Using (1) and (2) the measured S-parameters are finally converted to

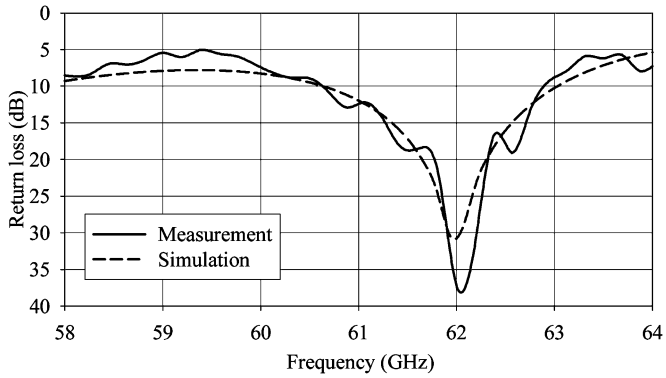

Fig. 5. Measured and simulated return loss.

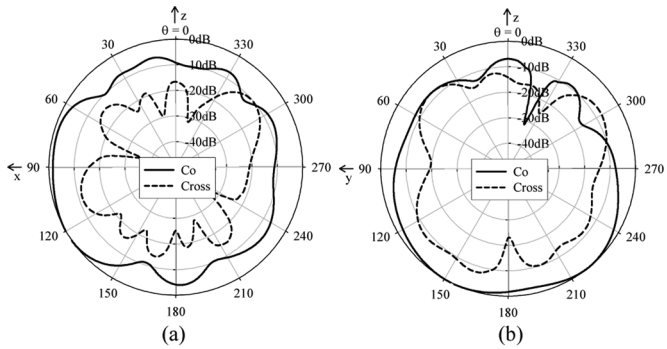

Fig. 6. Simulated radiation patterns at 62 GHz: (a) xz plane ($\Phi = 0°$), and (b) yz plane ($\Phi = 90°$).

the return loss of the differential antenna. Owing to the equipment limit, no radiation pattern measurement was done.

Fig. 5 shows the impedance matching performance of the AiP. A good agreement between simulated and measured results is observed. The simulated return loss shows a 10-dB impedance bandwidth of 60.6–63 GHz and a 31 dB value at the resonance frequency of 62 GHz. The measured return loss shows a 10-dB impedance bandwidth of 2.3 GHz from 60.6–62.9 GHz and a 37.5 dB value at the resonance frequency of 62 GHz.

Fig. 6 shows the simulated normalized radiation patterns for the xz and yz planes at 62 GHz. It is observed that for both planes the cross-polarization radiations are weaker than co-polarization ones. For example, in the x direction of the xz plane the cross-polarization radiation is 15 dB weaker. For the xz plane the co-polarization radiation is stronger in the front hemisphere (in the x direction). The maximum radiation is in the 120° direction with a front-to-back ratio of about 10 dB due to that the reflectors lie under the driver and directors. However, for the yz plane the co-polarization radiation is stronger in the upper hemisphere (in the $-z$ direction). This is because the bottom ground reduces the backside radiation. The simulated peak gain and efficiency for the Yagi AiP at 62 GHz are 6 dBi and 93%, respectively. The above results indicate the good directional antenna performance of our designed Yagi AiP.

IV. CONCLUSION

A Yagi antenna implemented in a thin cavity-down CBGA package in LTCC technology was reported for highly integrated 60-GHz radios. The Yagi AiP has a measured 10-dB impedance bandwidth from 60.6–62.9 GHz, indicating an acceptable matching at these frequencies. It also achieves a peak gain of 6 dBi at 62 GHz.

REFERENCES

[1] S. K. Moore, "Cheap chips for next wireless frontier," *IEEE Spectrum*, pp. 8–9, Jun. 2006.

[2] B. Floyd, S. Reynolds, U. Pfeiffer, T. Beukema, J. Grzyb, and C. Haymes, "A silicon 60 GHz receiver and transmitter chipset for broadband communications," in *ISSCC Digest Tech. Papers*, Feb. 2006, pp. 184–185.

[3] B. Razavi, "A 60-GHz CMOS receiver front-end," *IEEE J. Solid-State Circuits*, vol. 41, pp. 17–22, Jan. 2006.

[4] Y. P. Zhang, L. H. Guo, and M. Sun, "On-chip antennas for 60-GHz radios in silicon technology," *IEEE Trans. Electron Devices*, vol. 52, pp. 1664–1668, Jul. 2005.

[5] K. T. Chan, A. Chin, Y. P. Chen, Y. D. Lin, T. S. Duh, and W. J. Lin, "Integrated antennas on Si, proton-implanted Si and Si-on-quartz," in *IEDM Tech. Digest*, Jan. 2001, pp. 903–906.

[6] J. G. Kim, H. S. Lee, H. Lee, J. B. Yoon, and S. Hong, "60-GHz CPW-FED post-supported patch antenna using micromachining technology," *IEEE Microw. Wireless Compon. Lett.*, vol. 15, no. 10, pp. 635–637, Oct. 2005.

[7] U. R. Pfeiffer, J. Grzyb, D. Liu, B. Gaucher, T. Beukema, B. A. Floyd, and S. K. Reynolds, "A chip-scale packaging technology for 60-GHz wireless chipsets," *IEEE Trans. Microw. Theory Tech.*, vol. 54, no. 8, pp. 3387–3397, Aug. 2006.

[8] [Online]. Available: http://www.remcom.com/xfdtd

[9] Y. P. Zhang, "Integration of microstrip antenna on cavity-down ceramic ball grid array package," *Electron. Lett.*, vol. 38, no. 22, pp. 1307–1308, 2002.

[10] R. Meys and F. Janssens, "Measuring the impedance of balanced antennas by an S-parameter method," *IEEE Antennas Propag. Mag.*, vol. 40, no. 6, pp. 62–65, 1998.

[11] T. Zwick, C. Baks, U. R. Pfeiffer, D. Liu, and B. P. Gaucher, "Probe based MMW antenna measurement setup," in *Proc. IEEE Antennas Propagation Soc. Int. Symp.*, Monterey, CA, Jun. 2004, vol. 1, pp. 747–750.

Radiation Q and Gain of TM and TE Sources in Phase-Delayed Rotated Configurations

Do-Hoon Kwon

***Abstract*—The radiation quality factor and gain of antennas are compared for two source configurations between TM/TE-only spherical mode radiation and combined $\mathrm{TM} + \mathrm{TE}$ mode radiation. It is shown that the change to the combined $\mathrm{TM} + \mathrm{TE}$ mode radiation can reduce the quality factor by up to 50% and increase the gain by maximum 3 dB simultaneously. The condition for maximum gain increase provides a guideline for antenna designs for successfully achieving wide bandwidths and small sizes at the same time.**

***Index Terms*—Antenna gain, antenna miniaturization, directive antennas, radiation quality factor.**

I. INTRODUCTION

Relations among and limits upon the antenna size, bandwidth, efficiency, and gain have been investigated with respect to the radiation quality factor Q expressed in terms of spherical vector wave expansions [1]. In those analyses, the impedance bandwidth of an antenna was interpreted as a reciprocal of Q. Theoretical lower limits on the antenna Q were discussed for omni-directional and directive antennas in [2]–[7]. Practical upper limits on the antenna gain were also presented as a function of the antenna size [2], [3], [7], [8]. It was observed that antennas exciting the TM and TE (to r) modes of equal strengths have higher maximum achievable gains and smaller radiation Q's compared with antennas radiating either the TM or TE modes only.

Devising appropriate radiator structures and feeder configurations to excite both types of spherical modes is a reasonable design strategy to arrive at miniaturized antennas without compromising gains. There have been several antenna designs that specifically target simultaneous excitations of the TM and TE modes. For example, modified versions of conventional TEM horn antennas were developed with improved radiation efficiencies [9]–[11] in the low-frequency range. Combined electric and magnetic dipole antennas for electromagnetic pulse sensing applications were reported in [12], [13]. Low-profile wide loop antennas were demonstrated to have the maximum gain higher than that of a uniform line source of the same size over a wide frequency band [14]. The latter is known as the normal gain [2] for omnidirectional antennas, and it represents the practical upper limit on the gain without compromising bandwidth. Small printed ultrawideband antennas designed according to the above principle were presented in [15].

Although the antenna Q and the gain properties are known for both source configurations, no reports explicitly compare the two performance quantities when the source is switched between the TM/TE (TM or TE) and the $\mathrm{TM} + \mathrm{TE}$ configurations. Comparisons were made between the lowest-order TM/TE and $\mathrm{TM} + \mathrm{TE}$ modes in [16]. It was observed that a simultaneous excitation of the lowest-order $\mathrm{TM} + \mathrm{TE}$ modes reduces the antenna Q and a maximum gain increase of 3 dB can be achieved at the same time. This paper generalizes the previous analysis to higher order modes; the two quantities are compared between general TM/TE-only and $\mathrm{TM} + \mathrm{TE}$ source configurations. The sources radiating the TM and the TE modes in the $\mathrm{TM} + \mathrm{TE}$ configuration are allowed to have a phase difference and to be in a rotated position from each other. The maximum gain increase that can be obtained by the $\mathrm{TM} + \mathrm{TE}$ configuration is analyzed in terms of the desired polarization, the phase difference and the rotation angle between the TM and TE sources.

II. DECREASE IN RADIATION Q

The radiation quality factor Q of an antenna is generally defined as [3]

$$Q = \begin{cases} \frac{2\omega W_e}{P_r}, & W_e \geq W_m \\ \frac{2\omega W_m}{P_r}, & W_e \leq W_m \end{cases} \tag{1}$$

where P_r is the radiated power, W_e and W_m are the time-average electric and magnetic energies stored around the antenna. When computing Q, parts of the energies inside the smallest hypothetical sphere of radius a circumscribing the antenna are ignored such that the value of Q in (1) represents the minimum possible value. If $W_e \neq W_m$, an external reactive component is assumed to bring the antenna to resonance. The reciprocal of Q is usually interpreted to approximately represent the fractional antenna bandwidth.

Let a combination of electric and magnetic sources $(\mathbf{J}_a, \mathbf{M}_a)$ radiate TM spherical mode fields at the angular frequency ω. Outside the sphere of radius a, the associated electric field $\mathbf{E}_{\mathrm{TM}}$ can be expressed as

$$\mathbf{E}_{\mathrm{TM}} = \sum_{n=1}^{\infty} \sum_{m=0}^{n} B_{e_{omn}} \mathbf{N}_{e_{omn}} \tag{2}$$

Manuscript received April 27, 2007; revised October 7, 2007. Published August 6, 2008 (projected).

The author was with the Department of Electrical Engineering, The Pennsylvania State University, University Park, PA 16802 USA. He is now with the Electrical and Computer Engineering Department, University of Massachusetts Amherst, Amherst, MA 01003 USA (e-mail: kwon22@ieee.org).

Digital Object Identifier 10.1109/TAP.2008.924747